A structural model of the inactivation gate of voltage activated potassium channels

Ariela Vergara-Jaque[1,2,3+], Francisco Palma-Cerda[4+], Adam S. Lowet[4], Angel de la Cruz Landrau[4], Horacio Poblete[1,2,3], Alexander Sukharev[4], Jeffrey Comer[3*], and Miguel Holmgren[4*]

[1]Multidisciplinary Scientific Nucleus. Center for Bioinformatics and Molecular Simulation, Universidad de Talca, 2 Norte 685, Talca, Chile.

[2]Millennium Nucleus of Ion Channels-associated Diseases (MiNICAD), Chile.

[3]Institute of Computational Comparative Medicine, Nanotechnology Innovation Center of Kansas State, Department of Anatomy and Physiology, Kansas State University, Manhattan, Kansas 66506, USA.

[4]Molecular Neurophysiology Section, National Institute of Neurological Disorders and Stroke, National Institutes of Health, Bethesda, Maryland 20892, USA.

[+] These authors contributed equally to this work.

[*] Correspondence and requests for materials should be addressed to: **J.C.** Institute of Computational Comparative Medicine, Nanotechnology Innovation Center of Kansas State, Department of Anatomy and Physiology, Kansas State University, Manhattan, Kansas 66506, USA. E-mail: jeffcomer@ksu.edu. Telephone: +1-(785) 532-6311, or **M.H.** Molecular Neurophysiology Section, National Institute of Neurological Disorders and Stroke, National Institutes of Health, Bethesda, Maryland 20892, USA. E-mail: holmgren@ninds.nih.gov. Telephone: +1-(301) 451-6259.

Abstract

After opening, the *Shaker* voltage-gated potassium (K_V) channel rapidly inactivates when one of its four N-termini enters and occludes the channel pore. While it is known that the tip of the N-terminus reaches deep into the central cavity, the conformation adopted by this domain during inactivation and the nature of its interactions with the rest of the channel remain unclear. Here, we use molecular dynamics simulations coupled with electrophysiology experiments to reveal the atomic-scale mechanisms of inactivation. We find that the first six amino acids of the N-terminus spontaneously enter the central cavity in an extended conformation, establishing hydrophobic contacts with residues lining the pore. A second portion of the N-terminus, consisting of a long 24 amino acid α-helix, forms numerous polar contacts with residues in the intracellular entryway of the T1 domain. Double-mutant cycle analysis revealed a strong relationship between predicted interatomic distances and empirically observed thermodynamic coupling, establishing a plausible model of the transition of K_V channels to the inactivated state.

Introduction

Voltage-gated potassium channels are integral membrane proteins that function as homotetramer complexes (1, 2). The particular firing properties of neurons depend in part on the dynamics of gates within the K_V channels, which control permeation through a K^+ selective pore (3). In response to depolarization, all K_V channels open an intracellular gate that allows K^+ to permeate (4–6). In some K_V channels, including the *Shaker* channel from *Drosophila melanogaster* (2), opening the voltage-dependent gate leads to a rapid inactivation process produced by another gate, termed the inactivation particle or inactivation gate. This inactivation domain is located at the N-terminus of the channel (7, 8), and under certain stimuli enters deep into the central cavity, cutting off ion conduction (9, 10). The

inactivation mechanism is coupled to the activation process (7), and once the channel is open the inactivation gate acts like an open-channel blocker (11). Since *Shaker* K_V channels are homotetramers, each channel has four N-termini; however, only one of these is necessary to occlude the pore and cause inactivation (12, 13). The inactivation particle is highly disordered, which makes it not amenable to x-ray crystallography (6) or cryo-electron microscopy; therefore, the question arises of how such a disordered polypeptide is able to reliably and rapidly induce inactivation. Recent functional studies have revealed several key components of the inactivation mechanism, which requires that the cytoplasmic N-terminus be guided through the intracellular vestibule and where it then penetrates into the channel pore. During the first stage of inactivation, the N-terminus appears to interact with the T1 domain at the entryway to the intracellular vestibule on its way to the central cavity (14, 15). Once inside the central cavity, the tip of the N-terminus experiences hydrophobic interactions with residues lining the pore, blocking the permeation pathway (9, 10).

Despite this body of research, the precise interactions governing the transition of the N-terminus from the cytoplasm to the central cavity of the channel, as well as the conformational state that it adopts upon reaching the pore, have remained unclear. A β-hairpin conformation spanning residues 1 to 12 has been previously proposed (16, 17) for the N-terminus, with the hairpin loop (residues 6 and 7) forming its front end. However, mutagenesis experiments revealed contact between residue at the position 2 of the N-terminus and residue 470 within the central pore (9, 10), which appears inconsistent with this β-hairpin structure. In this study, we describe molecular modeling, molecular dynamics simulations (MD), and experimental mutant cycle analyses (18–20) to characterize the *Shaker* inactivation mechanism at the molecular level. The computational methods reveal a plausible conformation for the N-terminus during inactivation and identify several contacts between this domain and residues in the central pore and T1 domain. Mutant cycle analyses provide experimental support for the existence of these contacts.

Results

Difficulties of the β-hairpin model. The conformation adopted by the N-terminus during inactivation of the *Shaker* K_V channel has been controversial. Early efforts suggested that the inactivation particle acquires a β-hairpin structure (16), a proposal that was subsequently supported by a combination of electrophysiology, nuclear magnetic resonance, Fourier transform infrared spectroscopy and molecular dynamics (17, 21) . However, these structural studies were performed with peptides embedded in lipid bilayers or interacting with bacterial KcsA channels in the presence of detergent, which may not favor the same structure as is found within the pore of intact K_V channels. Subsequent mutagenesis experiments demonstrated that residue A2 of the N-terminal tip makes contact with residue I470 inside the central cavity (9). This finding appears to preclude a β-hairpin motif, which predicts that residue L7 enters more deeply than A2, impeding contact of the latter with I470. Based on that observation, our overall goal was to define the specific conformation adopted by the N-terminus during inactivation of the *Shaker* K_V channel and to characterize the nature of the interactions that allow for channel block.

To begin, we built a molecular model of the *Shaker* K_V channel on the basis of the K_V 1.2 crystal structure (22) with the pore in the open state. Because both channels exhibit a considerable sequence identity of 75%, our model is expected to have a correct fold and high accuracy in the atomic details. The 20 amino acid-long β-hairpin structure (17) was then docked onto the channel's intracellular vestibule, resulting in the structural model shown in Fig. 1*A*. The complex was relaxed in a 152 ns MD simulation. During this time, the β-hairpin made no progress in penetrating the central cavity. Therefore, to coax the positively charged N-terminal methionine to penetrate the central cavity, a membrane potential of 1.0 V was applied, and additional 227 ns of MD were run. Even though intracellular K^+ ions

could reach the selectivity filter under these conditions, the amino acids forming the β-hairpin did not penetrate the central cavity. Analysis of pore radius showed values of ≈5 Å in the region surrounding residue I470 (Fig. 1B). On the other hand, largest cross section of the β-hairpin along its axis exhibited a maximum radius of ≈7 Å, which occurs at the base of the hairpin (residues M1 and E12) and coincides with a distance of 5.3 Å between the C_α atoms of these residues (Fig. 1C). Structures of potassium-selective ion channels in open-pore conformations exhibit radii values < 6 Å (23), which makes the distortions of the inner vestibule necessary to accommodate a β-hairpin structure unlikely. In fact, during the simulation, we observed partial unzipping of the hairpin (reaching 12.9 Å between the C_α atoms at the base) and its migration away from the inner pore. These analyses therefore appear to exclude an inactivation particle with a β-hairpin conformation.

The helix-extension model. We propose a model in which the inactivation particle enters the inner vestibule as an extended structure so that the tip of the N-terminus can reach the central cavity. Secondary structure predictions using different algorithms (Fig. S1), applied to the full-length *Shaker* sequence, show mostly an α-helical structure from residues 11 to 54. For the first 10 residues of the N-terminus, however, the algorithms predicted a small α-helical portion or a disordered coil in free solution, rather than a β-hairpin. We then generated a *de novo* model of the first 36 amino acids of the *Shaker* K_V channel's N-terminus using the PEP-FOLD3 server (24). This structure was subsequently corroborated in the context of the Rosetta FlexPepDock protocol (25) (Fig. S2). The model contains a short α-helix (residues 1 to 8) followed by a longer α-helix (residues 12 to 36). As shown in Fig. 2A, this structure was placed in the channel's intracellular vestibule using computational docking and MD simulation. Within the first 50 ns of simulation, the short α-helix spontaneously began to unfold, and by 368 ns it had completely unfolded and begun to penetrate the central cavity in the absence of any external

forces (Fig. 2B). Penetration of an extended initial model of the N-terminus tip was also evaluated, nevertheless, it exhibited too much flexibility and failed to enter the pore. Recent studies have demonstrated that the tip of the N-terminus establishes direct contact with residues lining the central cavity's surface (9, 10). We used the distances between the C_α atoms of residue A2 of the N-terminus and the four I470 residues of the central cavity of the channel to quantify the degree of penetration and found that these distances decreased as the N-terminus began to penetrate the central cavity (Fig. 2*D*). However, after ≈170 ns, there were no further changes in the position of the inactivation particle. At the end of 368 ns simulation period, the distances between A2 and the four I470 residues in the central cavity were too long to be compatible with disulfide bond formation (≈ 7 Å), as is known to occur when these two residues are mutated to cysteines (9).

It is possible that further penetration of the N-terminus into the central cavity could happen spontaneously at 0 V on longer timescales, such as the millisecond timescale that characterizes wild-type *Shaker* inactivation. However, due to the computational cost of significantly longer simulations at the present time, we instead opted to apply an electric potential to promote further penetration of the N-terminal tip. Experimentally, the voltage has minimal intrinsic influence on the process of inactivation (26, 27). Nonetheless, our model predicts that the protonated primary amino group of the N-terminal methionine is affected by the membrane potential as compared with similar simulations having this group acetylated, where penetration of the N-terminus tip was not observed. It should be noted that these effects may become especially apparent at non-physiological voltages. Beginning from the final state of the 368 ns simulation at 0 V (Fig. 2B), we applied an electric potential of 0.6 V and simulated the system for additional 1.45 μs (Fig. 2C). This manipulation was intended to reduce barriers for penetration of the NH_3^+ terminal group into the central cavity. After about 570 ns of simulation (Fig. 2E**,** dashed line), the tip of the N-terminus entered deep into the central cavity and residue A2 made contact with residue I470 at distances suitable for disulfide bond formation (≈ 3.5 Å), as previous experiments have demonstrated

(9, 10). Despite the large voltages used in the simulation to observe the full penetration of the inactivation particle, the configuration obtained in this way might be physiologically relevant. To further test this notion, we performed an additional simulation to see whether the configuration was stable in the absence of an external voltage. Beginning from the final frame of the 1.45 μs simulation with 0.6 V applied, the transmembrane voltage was removed and an additional 270 ns of MD at 0 V were run. As expected, the inactivation particle remained in the pore, suggesting that the configuration of the inactivation particle was stable in the absence of an external voltage (Fig. S3).

Interestingly, the N-terminus tip was free to rotate inside the central cavity of the channel, and the residue A2 intermingled with various subunits, which is consistent with previous experiments (15). As can be seen in Fig. 2E, the N-terminus initially made contact with residue I470 of subunit A during the period 570–710 ns. Shortly afterward, the contact switches to residue I470 of subunit D (710–840 ns), and then to subunit C and back to subunit D again (840–950 ns). At this point, the tip of the inactivation gate penetrated even further into the central cavity, so the distances between A2 and all four I470 increased slightly. Additionally, in what may represent the fully inactivated state of *Shaker* K_V channel, K^+ ions were expelled from the selectivity filter (Fig. 2C). C-type inactivation in K_V channels depends on ion occupancy and permeation (28, 29). Structural features of the region surrounding the selectivity filter in our open-inactivated state of the channel are consistent with C-type inactivation (Fig. S4), although this may be attributed to the conditions of particularly high transmembrane voltages used in this study.

Specific interactions between the N-terminus structural model and the channel. Once the tip of the N-terminus entered the central cavity, the protonated amino group of the N-terminal methionine made close contact with the polar side chains of the T442 residues at the entrance of the selectivity filter (Fig. 3A). Furthermore, residues A2, A3, V4, A5 and L7 of the N-terminus established hydrophobic

interactions with residues V467, I470, A471, V474 and V478 of the permeation pathway, as has been previously proposed based on experimental data (9, 10, 15). González et al. reported a hydrophobic contact between residues A2 and I470 (9), whereas A3 was suggested to make contact with residues V474 and V478, which are homologues to V558 and V562 that make contact with the residue at position 3 of the inactivation particle in $K_V\alpha1.4$ (10). Both interactions are supported by our model (Fig. S5). Additionally, Y8 exhibited a hydrogen bond with N482 at the cytoplasmic entrance to the channel pore, potentially stabilizing the inactivation particle in the bound state.

The long α-helix between residues 12 and 36 made many contacts with residues located at the intracellular entryway of the permeation pathway (Fig. 3A,B). Specifically, polar interactions were identified between the residues D13, R17, K19 and R164, D193, E194, S479 of subunit D; and E35–K198 of subunit C. A hydrophobic interaction between Q25 and L170 was also found. All these interactions are summarized in Fig. 3C, which shows a contour-like map of the average distances (up to 15 Å; full penetration period) between residues of the N-terminus structural model and each of the four subunits of the channel. On a general level, our model predicts that the *Shaker* K_V channel's inactivation mechanism is mostly regulated by three components: 1) residues 2–7 of the N-terminus making hydrophobic contacts with residues in the central cavity, (2) Y8 establishing a break between the hydrophobic and polar region through a hydrogen bond with N482 and, 3) the long α-helix (residues 12–36) forming polar interactions with residues at the inner pore and T1 domain.

Experimental validation of the proposed structural model of the inactivation gate. The interactions between residues of the pore and the first 2–7 residues of the inactivation gate have been previously studied by mutant cycle analysis (10) and cysteine mutagenesis followed by chemical modification and disulfide bond formation (9). In addition, mutagenesis assays of charged residues in the T1 domain

revealed that the access of the tip of the N-terminus into the inner pore occurs through the side windows, located between the intracellular vestibule surface and the T1 domain (30, 31). A specific electrostatic interaction between the positively charged residue R18 of the inactivation particle and the negatively charged residues EDE161–163 in the T1 domain was found in *Aplysia* K_V channels (14), as well as between their homologs R17 and EDE192-194 in *Shaker* K_V channels (15). The novel interactions predicted by our model between the long α-helix (residues 12 to 36) and the T1 domain provide therefore an unique opportunity to extend these empirical studies more broadly.

To quantify the interactions predicted by MD simulations and validate our model, we used double-mutant cycle analysis (18, 19). A total of eight pairs from the putatively interacting residues (long α-helix/T1 domain) were selected, for which the predicted distances between the amino acids' side chains ranged from 3.6 to 14.6 Å. In addition, we studied the potential interaction between two pairs: 1) Y8 and N482, at the cytoplasmic end of the inner pore, for which a hydrogen bond interaction was identified, and 2) K19 and S479, establishing polar interaction (Fig. 3A-C). The distances along the MD simulation trajectories for these ten pairs of residues are shown in supplementary Figure S6. The trajectories show substantial dynamics of the inactivation gate outside of the intracellular cavity. Interestingly, Y8 maintained close interactions with N482 throughout most of the full penetration period, while transitioning between three different subunits of the channel. A representative example of the double-mutant cycle assays performed to evaluate interaction between pairs is shown in Fig. 4, The current recordings for D13/R164 are detailed. Each trace is a single current recording in response to a voltage step from −80 to +60 mV. Red lines overlapping the current recordings represent fits of the ionic current data to a Markov model for which the rate constants k_{on} and k_{off} of the inactivation process are the only free parameters (15). From these rates, we calculated the equilibrium constant (K_{eq}) of each construct and used them to estimate the degree of thermodynamic coupling between residues (Ω; see

Methods). A Ω value deviated from unity indicates an interaction. For D13/R164, the Ω value was 0.2 demonstrating a close contact between the two residues. SI *Table* I shows the average K_{eq} values of all single and double mutants analyzed in this study. Using the K_{eq} values, we calculated Ω for the ten selected pair of residues. For those instances in which the value was less than 1 we calculated the reciprocal and plotted them against the average distance between the side chains of each pair predicted from MD simulations (Fig. 5). Clearly, the Ω values drop sharply to unity as the simulation-derived distance between the two amino acids increased beyond ~5 Å, as would be expected for a direct intermolecular interaction. Interestingly, for those pairs in which the average distances were around 4 Å, their corresponding Ω values varied from ~2 to ~5. This apparent lack of correlation may originate from the fact that the kinetics of inactivation is governed by multiple interactions at multiple locations on the protein, and the chemical nature of the interactions between each pair is not the same. Thus, while predicted distances less than 5 Å should give rise to Ω values significantly different from unity, the model makes no strong predictions about their relationship within this limited range. In contrast, it makes a very strong prediction that residues above some critical distance threshold should have no measurable interaction. This prediction is supported by the data, validating the inactivation mechanism suggested by our model.

Discussion

Past experiments have identified the N-terminus as the inactivation gate of *Shaker* K_V channels (7, 8) and demonstrated several interactions between this domain and residues in the central cavity (9, 10, 32) and T1 domain (14, 15). However, these studies have failed to identify the atomic-scale mechanisms of inactivation as well as the conformation adopted by the N-terminus as it transitions from the intracellular space to the channel pore. Here, we used MD simulations alongside electrophysiological recordings to

address these questions. Our study argues against a β-hairpin motif inactivating the channel, mainly because experiments have shown close contact between A2/I470 in the channel pore (9), and analyses of the internal geometry of the permeation pathway in different Kv channels (23) show insufficient space to accommodate such deep penetration of the β-hairpin. Our data instead support a model of the inactivation gate as an extended peptide between residues 1–8, followed by a long α-helix from residues 12–36. In line with previous findings (9, 10, 32), our model identifies numerous hydrophobic contacts between the extended peptide and the amino acids of the central cavity and inner pore, terminating with a hydrogen bond between Y8 and N482 at the base of the pore. The long α-helix, in turn, serves to stabilize the inactivation particle at the level of the T1 domain through electrostatic interactions. These stabilizing contacts were confirmed by demonstrating a tight correspondence between the interatomic distances predicted by our model and the degree of thermodynamic coupling observed experimentally. This conformational ensemble is consistent with previous reports that the inactivation particle enters the pore through the intracellular entryway above the T1 domain (14, 15), but it goes further than any prior study by showing precisely where and how such a transition may take place.

Once the channel is blocked, our simulations corroborate the conclusion of previous experiments that the inactivation particle interacts with the four I470 residues in the central cavity with equal probability (15). Moreover, MD simulations of the N-terminus with the M1 residue acetylated showed no deep penetration into the pore, suggesting that the N-terminal tip must be protonated in order to block the channel. This is consistent with the affinity of the central cavity for positively charged ions, like potassium (4) and quaternary ammonium derivatives (10), and rationalizes the functional similarity between the inactivation gate and open-channel blockers (11).

On the other hand, to comply with empirical constraints and allow the tip of the N-terminus to penetrate deeply into the central cavity, we found it necessary to apply a membrane potential of 0.6 V. However, it remains very plausible that such penetration could occur at physiological voltages on longer

timescales than those probed by the MD simulations. In fact, permanence of the open-inactivated state of the channel in absence of a transmembrane potential was demonstrated in our model, discarding the voltage effects in the inactivation mechanism. As computational efficiency and power improves, it will be important to confirm that this is true in the context of realistic physiological conditions. Though 0.6 V is substantially higher than the voltages typically applied in electrophysiological experiments, it is within the range of commonly used electric potentials to simulate membrane proteins (33, 34). Moreover, the fact that the N-terminus was prohibited from entering the channel pore while adopting a β-hairpin conformation, even at higher membrane potentials (1.0 V), casts doubt on the relevance of this structure for inactivation and suggests that a narrower single-stranded conformation of the N-terminus is necessary for full penetration into the channel pore.

Finally, it should be noted that the principal focus of this study was to describe the *Shaker* K_V channels inactivation mechanism in the open state of the protein; therefore, our analyses do not distinguish the location of the inactivation gate when the channel is closed. However, it is tempting to speculate that many of the same interactions, particularly those between the long α-helix and the T1 domain, also manifest while the channel is in the closed state. This might favor the localization of the N-terminus within the intracellular vestibule even before the channel is open and contribute to rapid inactivation upon opening of the pore. Moreover, taking into account the tetrameric architecture of Shaker KV channels, a plausible model of the closed state might have all four N-termini residing near the intracellular entryway of the T1 domain until opening occurs.

In conclusion, the present work reveals previously unknown interactions that the N-terminus of *Shaker* K_V channels establishes with residues lining the ion permeation pathway and with the cytoplasmic T1 domain. Conservation of key residues for anchoring of the N-terminus during inactivation of KV channels homologous to Shaker (Fig. S7) allows us to hypothesize similar functional roles and suggests the significance of this study beyond *Shaker*. Moreover, while the calculations

presented here have a number of limitations—the use of approximate structural models, representation of only the open state of the channel, and the absence of a large portion of the inactivation particle connecting the N-terminus with the T1 domain, they suggest the key interactions stabilizing the bound state of the inactivation particle and dictate the kinetics of *Shaker* K_V channel inactivation. An improved characterization of the operation of K_V channels should lead to a richer understanding of how neurons sculpt the shape and frequency of action potentials, as well as to help the development of new pharmaceutical strategies for the treatment of associated channelopathies.

Methods

Mutagenesis. Wild-type *Shaker* K^+ channel DNA was used as a template to introduce single and double mutations, which were produced using standard PCR techniques.

DNA expression. All channel DNAs were cloned into GW1-CMV (British Biotechnology) vectors and co-transfected with CD8 and SV40 DNAs into HEK293T cells (35) using electroporation (Nucleofector II, Amaxa Biosystems) system. After transfection, cells were cultured in DMEM with 10% FBS. Experiments were performed one day after transfection.

Experimental solutions and electrophysiological recordings. The intracellular solution was composed of (mM): 160 KCl, 0.5 $MgCl_2$, 1 EGTA and 10 HEPES (pH=7.4 with KOH). The extracellular solution contained (mM): 150 NaCl, 10 KCl, 1 $MgCl_2$, 3 $CaCl_2$, 10 HEPES (pH=7.4 with NaOH). Current recordings were obtained from inside-out excised patches, sampled at 100 kHz and filtered at 5 kHz using an Axopatch 200B amplifier (Axon Instruments). Data acquisition was performed using a Digidata 1440A AD/DA converter and Clampex software (Axon Instruments). Borosilicate glass

pipettes (Harvard Apparatus) were pulled (Sutter Instrument) to have 1.9–2.7 MΩ resistance. The experiments were performed at 21–23 ºC, and monitored using a thermocoupler (Thermometric) in the chamber.

Modeling and analysis of ionic currents. Traces were fit in Matlab with a Markov kinetic model to estimate the values of k_{on} and k_{off} (15). The equilibrium constant ($K_{eq} = k_{on}/k_{off}$) was determined for each mutant channel, and thermodynamic cycle analyses were used to quantify the level of interaction (Ω) between two amino acids as follows (18):

$$\Omega = \frac{K_{eq}^{(WT,WT)} \times K_{eq}^{(Mut,Mut)}}{K_{eq}^{(WT,Mut)} \times K_{eq}^{(Mut,WT)}}$$

An Ω value different from unity indicates interaction between two mutations.

Molecular modeling of *Shaker* K^+ channel. A *Shaker* comparative model (residues 96 to 489) was built using the Kv1.2 channel from *Rattus norvegicus* (PDB ID 3LUT) (22) as a template. A preliminary pairwise sequence alignment for modeling, initially of only one monomer, was generated using the AlignMe server (36). This alignment was subsequently replicated to build a molecular model of the tetrameric channel structure. Adjustments in the initial alignment were made, and refined models were built to optimize agreement with PSIPRED (37, 38) secondary structure and TOPCONS (39) transmembrane topology predictions. In the final alignment, 74.7% of the residues were identical, and the similarity reached 83.4%. A total of 2000 iterations of model building were performed with MODELLER (40) applying symmetry restraints between the C_α atoms of each monomer. The best *Shaker* model was selected as that with the lowest Molpdf energy value in MODELLER and the highest Procheck (41) and global ProQM (42) scores. The final model is of excellent quality according to

Procheck, with 98.9% residues in the favored and additional allowed regions of the Ramachandran plot. The global ProQM score is also very high, with an optimal value of 0.614.

Prediction of the N-terminal segment folding. Secondary structure predictions of the full-length *Shaker* sequence (UniProt ID: P08510) were performed using the software PSIPRED (37, 38), SOPMA (43), SPIDER2 (44), JPRED4 (45) and PSSPRED (46). The PEP-FOLD server (24) was used to predict a *de novo* structural model of the inactivation particle, including the sequence of the first 36 amino acids of the protein (the maximum allowed by the software). A total of 200 models were generated, and we selected the one with the lowest sOPEP energy value in PEP-FOLD to use in our subsequent simulations.

Docking simulations. Docking simulations were carried out with a β-hairpin structure (PDB ID: 2LNY) (17) and the *de novo* predicted structural model of the inactivation particle. In preparation for docking, a grid box was built using the mass center of the four I470 residues of the homotetrameric model of the channel as a reference point. The grid was large enough ($47\times47\times47$ Å^3) to accommodate free motion of the N-terminus structural model into any region of the channel. The docking calculations were performed using AutoDock Vina (47) with the default scoring parameters, and AutoDockTools (48) was used to select the lowest scoring conformation of the inactivation particle docking with the channel's inner pore and T1 domain. The best conformation of the complex containing the *de novo* predicted N-terminus model was corroborated using the Rosetta FlexPepDock protocol (25). Starting from an approximate specification of a peptide structure and its binding site, FlexPepDock performs simultaneous docking and folding taking into account the receptor surface. A total of 11,000 conformations were generated for this complex and compared with those obtained by AutoDock Vina (Fig. S2).

Molecular dynamics simulations. The lowest scoring conformation of the two complexes yielded by computational docking were used as the starting point for MD simulations. To reduce the computational expense, only the channel pore (residues 378 to 489) and the T1 domain (residues 142 to 199) were

included in the simulations. Each complex was embedded in a fully hydrated palmitoyl-oleyl-phosphatidyl-choline (POPC) bilayer solvated with explicit water molecules. Three K^+ ions were placed in the selectivity filter at K^+ binding sites S_0, S_2 and S_4, and two water molecules were placed at S_1 and S_3 (49). Potassium and chloride ions (0.15 M KCl) were added to the aqueous phase to mimic physiological ionic strength and to ensure charge neutrality. The protonation states of the residues at neutral pH were checked with the PropKa program (50). The M1 residue was considered protonated for the two N-terminal structures, although an acetylated state of the N-terminus for the α-helical conformation was also evaluated. The initial configuration of each system was optimized by means of 25,000 steps of energy minimization, followed by equilibration and relaxation in a 152–368 ns MD simulation at 298 K in the isobaric-isothermal ensemble. Soft harmonic constraints were applied to the protein and the ions of the selectivity filter during the first 15 ns of simulation, which were decreased gradually from 60 to 0 kcal mol^{-1} $Å^{-2}$ over this period. The distance between the center of mass of each T1 domain and the transmembrane region of the same subunit was restrained to 45 Å using the collective variable module (Colvars) (51). The center-of-mass distances of neighboring subunits of the T1 domain were also restrained to 24 Å. All molecular dynamics simulations were performed using the program NAMD v2.10 (52) and the CHARMM36 (53) force field. The temperature was maintained using a Langevin thermostat with a damping coefficient of 5 ps^{-1}. The pressure (1 atm) was maintained using the Langevin piston method (54). Long-range electrostatic interactions were computed using the particle-mesh Ewald summation method (55), with a smooth real-space cutoff applied between 8 and 9 Å. All covalent bonds involving hydrogen as well as the intramolecular geometries of water molecules were constrained using the SETTLE algorithm (56). The Verlet I r-RESPA multiple time-step integrator (57) was used with a time step of 2 fs for most interactions and 4 fs for long-range electrostatics.

Structural analyses of the complexes were performed using the program VMD (58) . The dimensions of the channel's pore were calculated with the HOLE program (59).

Applied voltage simulations. After equilibration and relaxation of the complexes, MD simulations applying constant electric fields perpendicular to the membrane plane were performed in order to represent transmembrane potentials (33, 34) of +0.6 V and +1.0 V. The simulations were continued with the applied voltages for 0.227–1.45 μs. Distances between the side chains of pairs of key residues were evaluated during the applied voltage simulations (full penetration period, Fig. S6). To evaluate the convergence of the simulation representing of the open-inactivated state of the channel, starting from the last frame of the trajectory at 0.6 V, the transmembrane potential was removed and an additional 270 ns of MD were run removing the transmembrane potential (0 V). Distances between the pairs of residues were again calculated and compared with those found in the simulation under voltage (Fig. S3).

Acknowledgments

The Intramural Section Program of the National Institute of Neurological Disorders and Stroke of the National Institutes of Health (NS002993) and NSF grant CHE-1726332, as well as Kansas Bioscience Authority funds to the Institute of Computational Comparative Medicine (ICCM) and Nanotechnology Innovation Center of Kansas State University (NICKS), supported this work. A.V-J. and H.P. thank FONDECYT research initiation grants #11170223 and #1171155, respectively. We would like to thank Deepa Srikumar for Molecular Biology assistance. The Millennium Nucleus of Ion Channels-Associated Diseases (MiNICAD) is a Millennium Nucleus supported by the Iniciativa Científica Milenio of the Ministry of Economy, Development and Tourism (Chile).

Author contributions

M.H., A.V-J. and J.C. conceived the project. A.V-J. and H.P. carried out computational modeling and simulations. J.C. supervised computational simulations efforts. F.P-C., A.S., A.C.L., A.S.L., and M.H. designed, performed and analyzed the experimental data. A.V-J., J.C., F.P-C, A.S.L. and M.H. wrote the manuscript. All authors contributed to the editing of the paper and scientific discussions.

References

1. MacKinnon, R. 1991. Determination of the subunit stoichiometry of a voltage-activated potassium channel. Nature. 350: 232–235.
2. Papazian, D.M., T.L. Schwarz, B.L. Tempel, Y.N. Jan, and L.Y. Jan. 1987. Cloning of genomic and complementary DNA from Shaker, a putative potassium channel gene from Drosophila. Science. 237: 749–753.
3. Yellen, G. 2002. The voltage-gated potassium channels and their relatives. Nature. 419: 35–42.
4. Doyle, D.A., J. Morais Cabral, R.A. Pfuetzner, A. Kuo, J.M. Gulbis, S.L. Cohen, B.T. Chait, and R. MacKinnon. 1998. The structure of the potassium channel: molecular basis of K+ conduction and selectivity. Science. 280: 69–77.
5. Liu, Y., M. Holmgren, M.E. Jurman, and G. Yellen. 1997. Gated Access to the Pore of a Voltage-Dependent K+ Channel. Neuron. 19: 175–184.
6. Long, S.B., E.B. Campbell, and R. Mackinnon. 2005. Crystal structure of a mammalian voltage-dependent Shaker family K+ channel. Science. 309: 897–903.
7. Hoshi, T., W.N. Zagotta, and R.W. Aldrich. 1990. Biophysical and molecular mechanisms of Shaker potassium channel inactivation. Science. 250: 533–538.
8. Zagotta, W.N., T. Hoshi, and R.W. Aldrich. 1990. Restoration of inactivation in mutants of Shaker potassium channels by a peptide derived from ShB. Science. 250: 568–571.
9. Gonzalez, C., A. Lopez-Rodriguez, D. Srikumar, J.J.C. Rosenthal, and M. Holmgren. 2011. Editing of human K(V)1.1 channel mRNAs disrupts binding of the N-terminus tip at the intracellular cavity. Nat. Commun. 2: 436.
10. Zhou, M., J.H. Morais-Cabral, S. Mann, and R. MacKinnon. 2001. Potassium channel receptor site for the inactivation gate and quaternary amine inhibitors. Nature. 411: 657–661.
11. Demo, S.D., and G. Yellen. 1991. The inactivation gate of the Shaker K+ channel behaves like an open-channel blocker. Neuron. 7: 743–753.
12. Gomez-Lagunas, F., and C.M. Armstrong. 1995. Inactivation in ShakerB K+ channels: a test for the number of inactivating particles on each channel. Biophys. J. 68: 89–95.

13. MacKinnon, R., R.W. Aldrich, and A.W. Lee. 1993. Functional stoichiometry of Shaker potassium channel inactivation. Science. 262: 757–759.
14. Prince-Carter, A., and P.J. Pfaffinger. 2009. Multiple intermediate states precede pore block during N-type inactivation of a voltage-gated potassium channel. J. Gen. Physiol. 134: 15–34.
15. Venkataraman, G., D. Srikumar, and M. Holmgren. 2014. Quasi-specific access of the potassium channel inactivation gate. Nat. Commun. 5: 4050.
16. Encinar, J.A., A.M. Fernández, E. Gil-Martín, F. Gavilanes, J.P. Albar, J.A. Ferragut, and J.M. González-Ros. 1998. Inactivating peptide of the Shaker B potassium channel: conformational preferences inferred from studies on simple model systems. Biochem. J. 331: 497–504.
17. Weingarth, M., C. Ader, A.S.J. Melquiond, D. Nand, O. Pongs, S. Becker, A.M.J.J. Bonvin, and M. Baldus. 2012. Supramolecular Structure of Membrane-Associated Polypeptides by Combining Solid-State NMR and Molecular Dynamics Simulations. Biophys. J. 103: 29–37.
18. Hidalgo, P., and R. MacKinnon. 1995. Revealing the architecture of a K+ channel pore through mutant cycles with a peptide inhibitor. Science. 268: 307–310.
19. Serrano, L., A. Horovitz, B. Avron, M. Bycroft, and A.R. Fersht. 1990. Estimating the contribution of engineered surface electrostatic interactions to protein stability by using double-mutant cycles. Biochemistry. 29: 9343–9352.
20. Carter, P.J., G. Winter, A.J. Wilkinson, and A.R. Fersht. 1984. The use of double mutants to detect structural changes in the active site of the tyrosyl-tRNA synthetase (Bacillus stearothermophilus). Cell. 38: 835–840.
21. Molina, M.L., F.N. Barrera, J.A. Encinar, M.L. Renart, A.M. Fernández, J.A. Poveda, J. Santoro, M. Bruix, F. Gavilanes, G. Fernández-Ballester, J.L. Neira, and J.M. González-Ros. 2008. N-type Inactivation of the Potassium Channel KcsA by the Shaker B "Ball" Peptide Mapping the Inactivating Peptide-binding Epitope. J. Biol. Chem. 283: 18076–18085.
22. Chen, X., Q. Wang, F. Ni, and J. Ma. 2010. Structure of the full-length Shaker potassium channel Kv1.2 by normal-mode-based X-ray crystallographic refinement. Proc. Natl. Acad. Sci. 107: 11352–11357.
23. Moldenhauer, H., I. Díaz-Franulic, F. González-Nilo, and D. Naranjo. 2016. Effective pore size and radius of capture for K(+) ions in K-channels. Sci. Rep. 6: 19893.
24. Thévenet, P., Y. Shen, J. Maupetit, F. Guyon, P. Derreumaux, and P. Tufféry. 2012. PEP-FOLD: an updated de novo structure prediction server for both linear and disulfide bonded cyclic peptides. Nucleic Acids Res. 40: W288–W293.
25. Raveh, B., N. London, L. Zimmerman, and O. Schueler-Furman. 2011. Rosetta FlexPepDock ab-initio: simultaneous folding, docking and refinement of peptides onto their receptors. PloS One. 6: e18934.
26. Zagotta, W.N., and R.W. Aldrich. 1990. Voltage-dependent gating of Shaker A-type potassium channels in Drosophila muscle. J. Gen. Physiol. 95: 29–60.
27. Zagotta, W.N., T. Hoshi, and R.W. Aldrich. 1989. Gating of single Shaker potassium channels in Drosophila muscle and in Xenopus oocytes injected with Shaker mRNA. Proc. Natl. Acad. Sci. U. S. A. 86: 7243–7247.
28. Boiteux, C., and S. Bernèche. 2011. Absence of ion-binding affinity in the putatively inactivated low-[K+] structure of the KcsA potassium channel. Struct. Lond. Engl. 1993. 19: 70–79.
29. Morales, M.J., J.O. Wee, S. Wang, H.C. Strauss, and R.L. Rasmusson. 1996. The N-terminal domain of a K+ channel beta subunit increases the rate of C-type inactivation from the cytoplasmic side of the channel. Proc. Natl. Acad. Sci. U. S. A. 93: 15119–15123.
30. Kobertz, W.R., C. Williams, and C. Miller. 2000. Hanging gondola structure of the T1 domain in a voltage-gated K(+) channel. Biochemistry. 39: 10347–10352.

31. Wang, W., J.K. Takimoto, G.V. Louie, T.J. Baiga, J.P. Noel, K.-F. Lee, P.A. Slesinger, and L. Wang. 2007. Genetically encoding unnatural amino acids for cellular and neuronal studies. Nat. Neurosci. 10: 1063–1072.
32. Bhalla, T., J.J.C. Rosenthal, M. Holmgren, and R. Reenan. 2004. Control of human potassium channel inactivation by editing of a small mRNA hairpin. Nat. Struct. Mol. Biol. 11: 950–956.
33. Gumbart, J., F. Khalili-Araghi, M. Sotomayor, and B. Roux. 2012. Constant electric field simulations of the membrane potential illustrated with simple systems. Biochim. Biophys. Acta. 1818: 294–302.
34. Roux, B. 2008. The Membrane Potential and its Representation by a Constant Electric Field in Computer Simulations. Biophys. J. 95: 4205–4216.
35. Jurman, M.E., L.M. Boland, Y. Liu, and G. Yellen. 1994. Visual identification of individual transfected cells for electrophysiology using antibody-coated beads. BioTechniques. 17: 876–881.
36. Stamm, M., R. Staritzbichler, K. Khafizov, and L.R. Forrest. 2014. AlignMe—a membrane protein sequence alignment web server. Nucleic Acids Res. 42: W246–W251.
37. Jones, D.T. 1999. Protein secondary structure prediction based on position-specific scoring matrices. J. Mol. Biol. 292: 195–202.
38. Buchan, D.W.A., F. Minneci, T.C.O. Nugent, K. Bryson, and D.T. Jones. 2013. Scalable web services for the PSIPRED Protein Analysis Workbench. Nucleic Acids Res. 41: W349-357.
39. Tsirigos, K.D., C. Peters, N. Shu, L. Käll, and A. Elofsson. 2015. The TOPCONS web server for consensus prediction of membrane protein topology and signal peptides. Nucleic Acids Res. 43: W401-407.
40. Eswar, N., B. Webb, M.A. Marti-Renom, M.S. Madhusudhan, D. Eramian, M.-Y. Shen, U. Pieper, and A. Sali. 2007. Comparative protein structure modeling using MODELLER. Curr. Protoc. Protein Sci. Chapter 2: Unit 2.9.
41. Laskowski, R.A., M.W. MacArthur, D.S. Moss, and J.M. Thornton. 1993. PROCHECK: a program to check the stereochemical quality of protein structures. J. Appl. Crystallogr. 26: 283–291.
42. Ray, A., E. Lindahl, and B. Wallner. 2010. Model quality assessment for membrane proteins. Bioinformatics. 26: 3067–3074.
43. Geourjon, C., and G. Deléage. 1995. SOPMA: significant improvements in protein secondary structure prediction by consensus prediction from multiple alignments. Comput. Appl. Biosci. CABIOS. 11: 681–684.
44. Yang, Y., R. Heffernan, K. Paliwal, J. Lyons, A. Dehzangi, A. Sharma, J. Wang, A. Sattar, and Y. Zhou. 2017. SPIDER2: A Package to Predict Secondary Structure, Accessible Surface Area, and Main-Chain Torsional Angles by Deep Neural Networks. Methods Mol. Biol. Clifton NJ. 1484: 55–63.
45. Drozdetskiy, A., C. Cole, J. Procter, and G.J. Barton. 2015. JPred4: a protein secondary structure prediction server. Nucleic Acids Res. 43: W389-394.
46. Yang, J., R. Yan, A. Roy, D. Xu, J. Poisson, and Y. Zhang. 2015. The I-TASSER Suite: protein structure and function prediction. Nat. Methods. 12: 7–8.
47. Trott, O., and A.J. Olson. 2010. AutoDock Vina: improving the speed and accuracy of docking with a new scoring function, efficient optimization and multithreading. J. Comput. Chem. 31: 455–461.
48. Morris, G.M., R. Huey, W. Lindstrom, M.F. Sanner, R.K. Belew, D.S. Goodsell, and A.J. Olson. 2009. AutoDock4 and AutoDockTools4: Automated docking with selective receptor flexibility. J. Comput. Chem. 30: 2785–2791.
49. Aqvist, J., and V. Luzhkov. 2000. Ion permeation mechanism of the potassium channel. Nature. 404: 881–884.

50. Olsson, M.H.M., C.R. Søndergaard, M. Rostkowski, and J.H. Jensen. 2011. PROPKA3: Consistent Treatment of Internal and Surface Residues in Empirical pKa Predictions. J. Chem. Theory Comput. 7: 525–537.
51. Fiorin, G., M.L. Klein, and J. Hénin. 2013. Using collective variables to drive molecular dynamics simulations. Mol. Phys. 111: 3345–3362.
52. Phillips, J.C., R. Braun, W. Wang, J. Gumbart, E. Tajkhorshid, E. Villa, C. Chipot, R.D. Skeel, L. Kalé, and K. Schulten. 2005. Scalable molecular dynamics with NAMD. J. Comput. Chem. 26: 1781–1802.
53. MacKerell, A.D., D. Bashford, M. Bellott, R.L. Dunbrack, J.D. Evanseck, M.J. Field, S. Fischer, J. Gao, H. Guo, S. Ha, D. Joseph-McCarthy, L. Kuchnir, K. Kuczera, F.T. Lau, C. Mattos, S. Michnick, T. Ngo, D.T. Nguyen, B. Prodhom, W.E. Reiher, B. Roux, M. Schlenkrich, J.C. Smith, R. Stote, J. Straub, M. Watanabe, J. Wiórkiewicz-Kuczera, D. Yin, and M. Karplus. 1998. All-atom empirical potential for molecular modeling and dynamics studies of proteins. J. Phys. Chem. B. 102: 3586–3616.
54. Feller, S.E., Y. Zhang, R.W. Pastor, and B.R. Brooks. 1995. Constant pressure molecular dynamics simulation: The Langevin piston method. J. Chem. Phys. 103: 4613–4621.
55. Essmann, U., L. Perera, M.L. Berkowitz, T. Darden, H. Lee, and L.G. Pedersen. 1995. A smooth particle mesh Ewald method. J. Chem. Phys. 103: 8577–8593.
56. Miyamoto, S., and P.A. Kollman. 1992. Settle: An analytical version of the SHAKE and RATTLE algorithm for rigid water models. J. Comput. Chem. 13: 952–962.
57. Tuckerman, M., B.J. Berne, and G.J. Martyna. 1992. Reversible multiple time scale molecular dynamics. J. Chem. Phys. 97: 1990–2001.
58. Humphrey, W., A. Dalke, and K. Schulten. 1996. VMD: Visual molecular dynamics. J. Mol. Graph. 14: 33–38.
59. Smart, O.S., J.G. Neduvelil, X. Wang, B.A. Wallace, and M.S. Sansom. 1996. HOLE: a program for the analysis of the pore dimensions of ion channel structural models. J. Mol. Graph. 14: 354–360, 376.

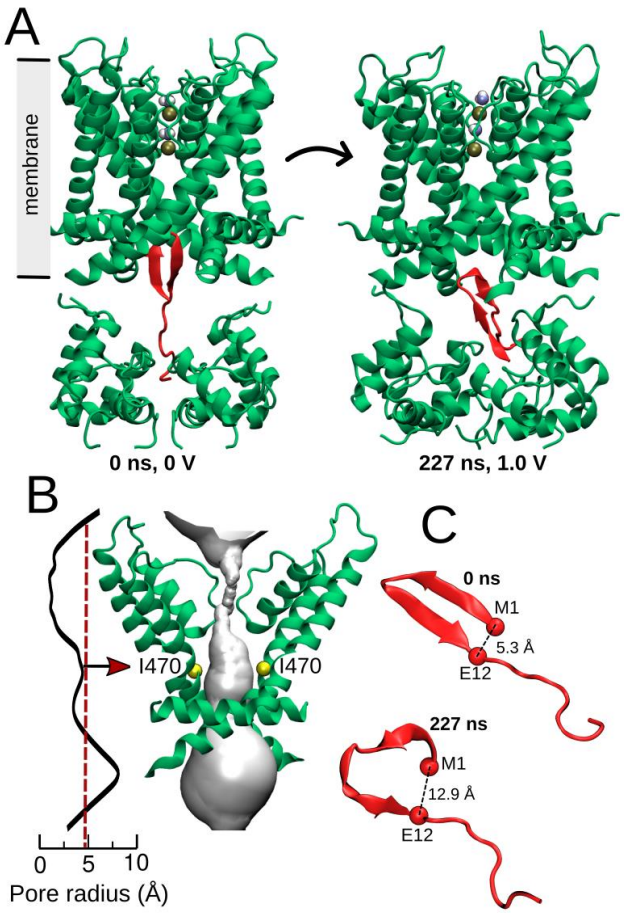

Figure 1. The central cavity has insufficient space to accommodate a β-hairpin structure. (A) Cartoon representation of *Shaker* K_V channel (green) in complex with the N-terminus (red) in a β-hairpin conformation. Potassium ions and water molecules in the selectivity filter are depicted with space-filling representations. The complex was embedded in a solvated membrane and simulated for 227 ns, applying a transmembrane potential of 1.0 V. (B) Pore-radius profile of the channel calculated as an average over the MD simulation. The initial non-equilibrium portion of the trajectory was discarded for the analysis. The HOLE pore-lining surface (gray) and channel pore (green) in the last frame of the MD trajectory are shown in the inset. The I470 residues are depicted as yellow spheres. (C) Initial (top) and final (bottom) conformation after simulation of the β-hairpin structure in the channel. The distance between the C_α atoms of the M1 and E12 residues indicates that the β-hairpin starts to open during the simulation.

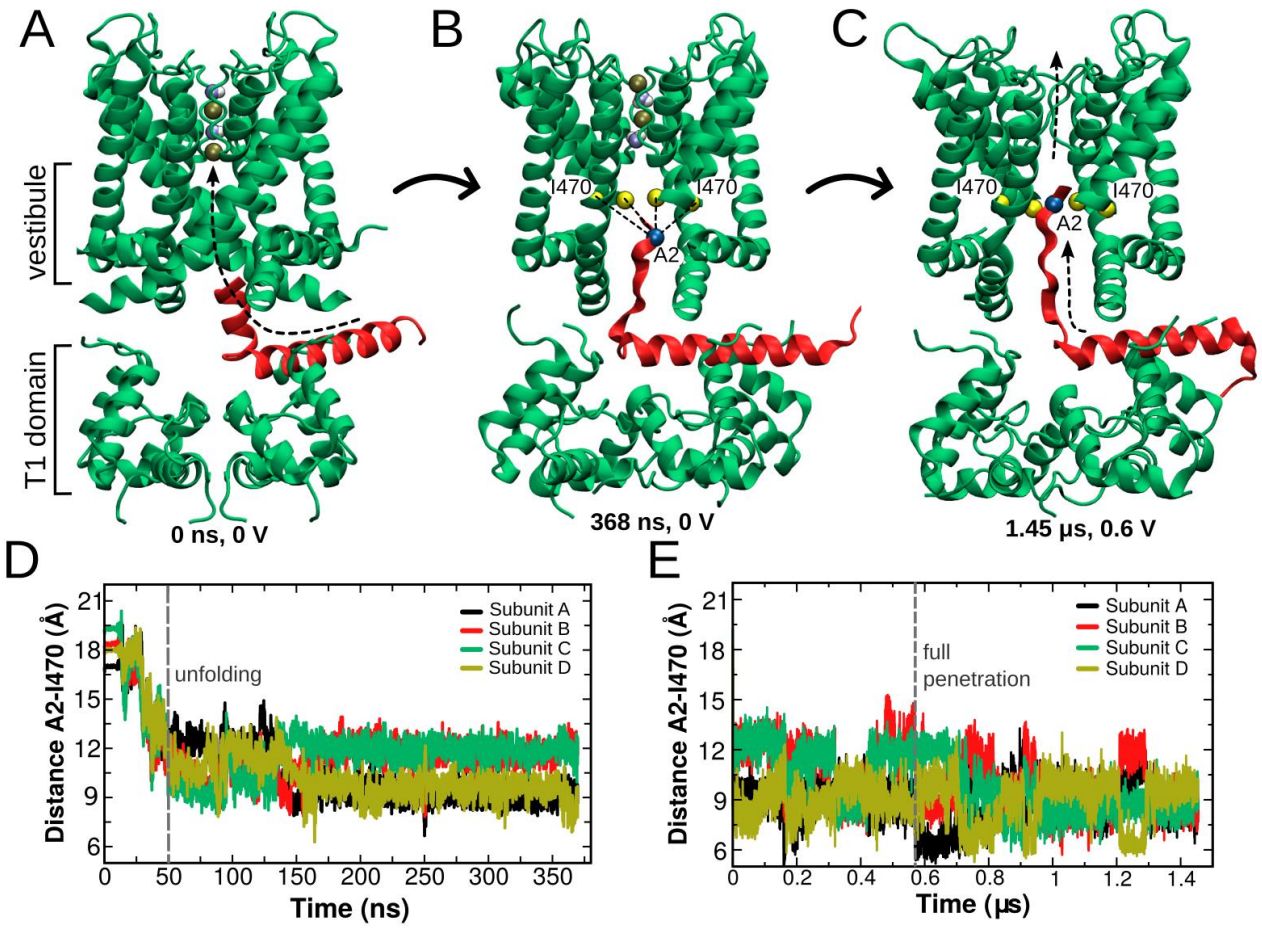

Figure 2. The N-terminus enters the inner vestibule as an unfolded structure. (A) Structure of the *Shaker* K_V channel (green) interacting with the double α-helical model of the inactivation particle (red). K^+ ions and water molecules within the selectivity filter are shown as spheres. The complex was embedded in a membrane solvated with explicit water molecules. (B) After 368 ns of MD simulation without an applied voltage, the tip of the N-terminus unfolds and partially penetrates the central cavity. Residues A2 and I470 are indicated by blue and yellow spheres, respectively. (C) Final state of the complex after 1.45 µs of simulation under a transmembrane potential of 0.6 V. The close contact between the residues A2 and I470 indicates full penetration of the N-terminus tip and, therefore, complete blocking of the channel. (D) Distance between the C_α atoms of the A2 residue of the N-terminus and the I470 residues of each channel subunit as a function of simulated time without an applied voltage. (E) Distance between the C_α atoms of residues A2 and I470 as a function of simulated time applying a voltage of 0.6 V.

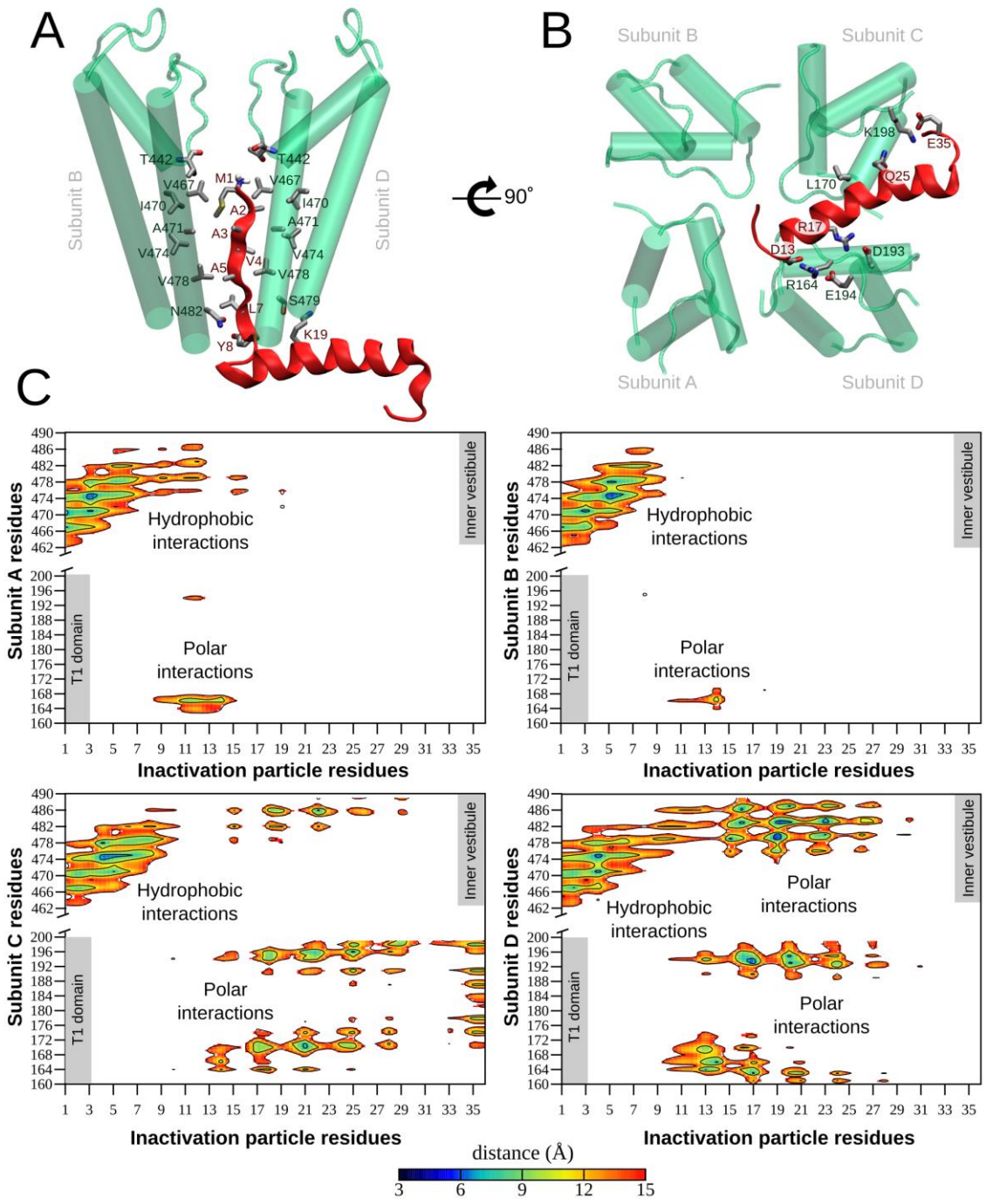

Figure 3. Association of the N-terminus with the channel is determined by both hydrophobic and polar components. (A) Simulation snapshot of the extended structure of the N-terminus making contact with residues in the central and inner cavity of *Shaker* K_V channel. The N-terminus (red) makes contact with all four subunits of the channel; however, for clarity only two subunits are shown in cartoon representation (green). The channel pore (segments S5 and S6) is oriented with the extracellular side on

top. (B) A rotation of 90° shows key contacts stabilizing the long α-helical portion of the inactivation particle in the intracellular entryway of the T1 domain. The residues in (A) and (B) are displayed as sticks colored by atom type – C in gray, O in red, N in blue and S in yellow. (C) Contour map representing the average distance between the center of mass of the residue's side chains of the N-terminus and the channel during the MD simulation (period of full penetration). The *x*-axis corresponds to residues in the inactivation particle, while the *y*-axis corresponds to residues in the T1-domain or inner vestibule. The color scale of the distances is ranged from 3 to 15 Å, with larger distances indicated by white.

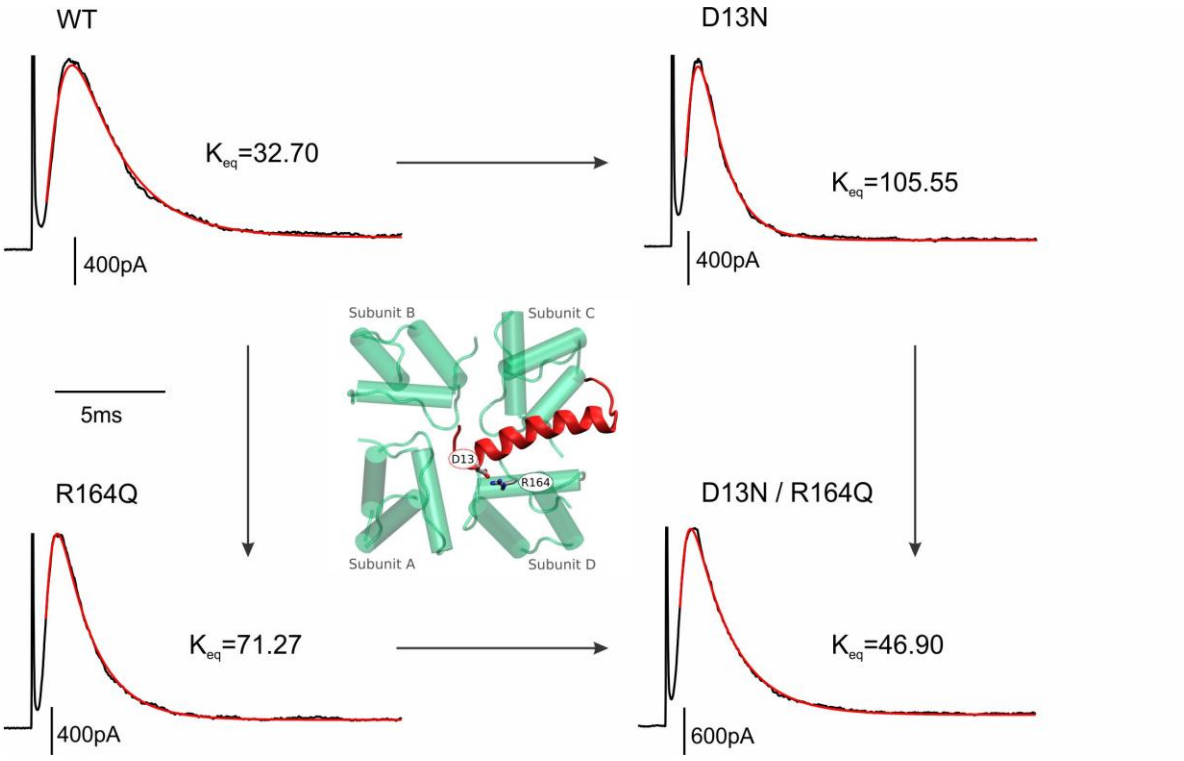

Figure 4. Thermodynamic coupling analysis between D13 and R164. Single current trace from wild-type (WT), single mutants (D13N and R164Q), and double mutant (D13N/R164Q) channels in response to a voltage step from –80 mV to +60 mV. Red lines overlying the traces represent the best fits of the data to an inactivation model. The equilibrium constants (K_{eq}) were estimated from the best-fit parameter values for k_{on} and k_{off}. The K_{eq} values correspond to estimations for each current trace. With these values, the estimated thermodynamic coupling coefficient (Ω) was 0.20 (see Methods). The center of the cycle shows the location of these two amino acids at the end of the MD simulation.

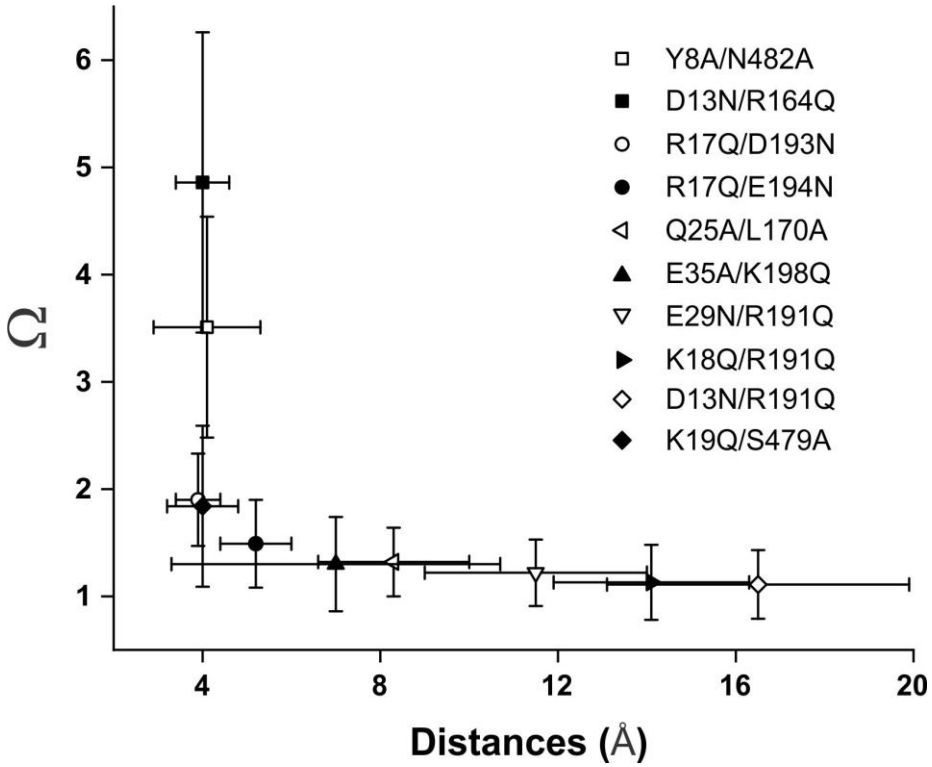

Figure 5. Relationship between thermodynamic coupling coefficients and distances. For those pairs in which the Ω value was less than 1, the reciprocal was plotted. Error bars on the y-axis represent the propagated SEM of the four K_{eq} estimations used to calculate each Ω value. Distances (x-axis) were measured between the atoms (residue1:atom and residue2:atom) Y8:OH and N482:Nδ2, D13:Cγ and R164:Cζ, R17:Cζ and D193:Cγ, K19: Nζ and S479:OG, R17:Cζ and E194:Cδ, E35:Cδ and K198:Nζ, Q25:Cδ and L170:Cγ, E29:Cδ and R191:Cζ, K18: Nζ and R191:Cζ, and D13:Cγ and R191:Cζ. Distance values represent the mean ± the SD of the entire "full penetration" period of the simulation, except for two cases in which the inactivation gate made contact with more than one subunit (see Figure S6). In those instances, the average distance and SD were calculated from a period in which contact was with a single subunit. For Y8-N482 pair, this period was between t=0.71 and 1.125 μs in contact with Subunit B. For the pair D13-R164, contact was with Subunit D between t=0.6 and 1.3 μs.